Supporting Information: Two-dimensional band structure in honeycomb metal-organic frameworks

Avijit Kumar,[†] Kaustuv Banerjee,[†] Adam S. Foster,[‡,¶,§] and Peter Liljeroth[*,†]

†*Department of Applied Physics, Aalto University School of Science, PO Box 15100, 00076 Aalto, Finland*

‡*COMP Center of Excellence, Department of Applied Physics, Aalto University, P.O. Box 11100, 00076 Aalto, Espoo, Finland*

¶*WPI Nano Life Science Institute (WPI-NanoLSI), Kanazawa University, Kakuma-machi, Kanazawa 920-1192, Japan*

§*Graduate School Materials Science in Mainz, Staudinger Weg 9, 55128, Germany*

E-mail: peter.liljeroth@aalto.fi

Methods

Sample preparation. The experiments were performed in an ultra-high vacuum system with a base pressure lower than 1×10^{-10} mbar. Ir(111) sample was cleaned by repetitive cycles of sputtering using high energy (2 kV) Ne beam and annealing in oxygen environment at 900 °C followed by flashing to 1300 °C. Graphene was grown by adsorbing ethylene and flashing the sample to 1100 - 1300 °C in a TPG (temperature programmed growth) step followed by a CVD step where the Ir(111) substrate at 1100 - 1300 °C is exposed to ethylene gas at 4×10^{-7} mbar pressure for around 60 s. This gives approximately a full monolayer coverage

of graphene (G/Ir(111)).

$DCBP_xCo_y$ structures were prepared by sequential deposition of the molecule and cobalt atoms on G/Ir(111) substrate at various temperatures. A submonolayer close-packed assembly of DCBP molecules was achieved by depositing it on G/Ir(111) substrate kept at room temperature using a home build evaporator at 47 °C. Addition of cobalt using a high-temperature effusion cell to the molecular assembly led to a spontaneous formation of $DCBP_4Co$ single complexes and $DCBP_3Co$ stripe-phase domains depending on the DCBP:Co stoichiometry. To synthesize $DCBP_3Co_2$ honeycomb MOF, cobalt was further added to the substrate at temperature 60 - 70 °C.

Similarly, DCA_xCo_y structures were prepared by sequential deposition of the molecule and cobalt atoms on G/Ir(111) substrate at various temperatures. Addition of cobalt to the submonolayer assembly of DCA molecules (evaporation temperature 60 °C) on G/Ir(111) substrate at room-temperature lead to spontaneous formation of assembly of DCA_3Co single complexes. To synthesize DCA_3Co_2 honeycomb MOF, cobalt was further added to the assembly of DCA molecules on G/Ir(111) substrate at ∼85 °C. Alternatively, substrate with assembly of DCA_3Co single complexes was annealed at temperature 80-90 °C for 45 minutes to form small domains of DCA_3Co_2 honeycomb MOF. Prolonged annealing at similar temperature increased the domain size.

STM and AFM experiments. STM and AFM experiments were carried out using a Createc low-temperature STM/AFM at a temperature of $T = 4.5$ K. $\mathrm{d}I/\mathrm{d}V$ spectra were acquired with lock-in detection using voltage modulation with amplitude of 10 - 15 mV. All STM and STS measurements on the MOFs have been carried out with metallic, non-functionalized tips unless stated otherwise. Non-contact AFM (nc-AFM) measurements were carried out using a qPlus sensor with resonance frequency $f_0 \sim 30.7$ kHz, a quality factor $Q \sim 10^5$, a spring constant $k \sim 1.8$ kN/m, and an oscillation amplitude of 50 pm. Here, the tips were functionalized by picking up individual CO molecules on a Cu(111) surface as described elsewhere.[S1] nc-AFM images were acquired in the constant height mode at a

sample bias of < 5 mV. WSxM[S2] and Gwyddion[S3,S4] software were used to process all the STM and nc-AFM images.

Computational methods. All first principles calculations in this work were performed using the periodic plane-wave basis VASP code[S5,S6] implementing the spin-polarized density functional theory (DFT). To accurately include van der Waals interactions in this system we used the optB86B+vdW-DF functional,[S7–S9] selected based on previous work showing that it provides a sufficiently accurate description for all subsystems involved in the measurement. Projected augmented wave (PAW) potentials were used to describe the core electrons,[S10] with a kinetic energy cutoff of 550 eV (with `PREC=accurate`). Systematic k-point convergence was checked for all systems, with sampling chosen according to system size. This approach converged the total energy of all the systems to the order of meV. Significantly increased k-point sampling with frozen geometries was used as the basis for the band structure calculations. The properties of the bulk graphite, graphene and the isolated molecular structures were carefully checked within this methodology, and excellent agreement was achieved with experiments where possible. For calculations of the network structures on graphene, system sizes were chosen to minimize lattice mismatch and any remaining strain (less than 1%) was accommodated in the graphene. Note that for calculations of the DCA molecular network on graphene, DFT consistently predicted that the three-fold symmetry seen experimentally would be broken by displacement of the Co closer to two of the nitrogens by about 0.02 Å. Although this is at the limits of our accuracy, we cannot exclude that in reality something else plays a role in maintaining the symmetry, for example the metal substrate. Since asymmetric structures were never observed experimentally, we constrained the system to be three-fold symmetric. On graphene, the calculations suggest displacement of Co towards the surface (larger than for $DCBP_3Co_2$), which is not really seen in the experiment. Symmetric and asymmetric systems had minor differences in their band structures, especially compared to those between antiferromagnetic and ferromagnetic cases. As a further check, we also performed calculations on a DCA_3Mn_2 framework using the same approach, and found very

similar results to those published previously.[S11]

DCA_3Co_2 spin stability. To explore the stability of the magnetic phases and give us more confidence in our choice for comparison to experiment, we calculated the DCA_3Co_2 network in both FM and AFM spin configurations using the LSDA+U approach[S12] for a variety of reasonable effective U values. This assumes that strong d-electron correlation plays a significant role in the favoured magnetic phase and this is not fully captured in our standard approach. Here we used the work of Mann *et al*[S13] as a guide for choice of U, with $U = 2.0 - 5.0$ eV suggested as reasonable for Co-based systems. As mentioned in the main text, at $U = 0$ eV we found that an AFM configuration was favoured by 0.05 eV. At $U = 2.0$ eV, the FM phase is now favoured by 0.11 eV and this increases to 0.21 eV at $U = 5.0$ eV, supporting our choice of the FM phase for comparison to experiment.

STM and AFM image simulations. STM images were calculated using the HIVE package.[S14] For calculated AFM images we used our implementation of the model developed by Hapala *et al.*[S15] The molecular structure was taken from DFT simulations and the electrostatic potential was extracted from the Hartree potential.[S15,S16] The mechanical AFM model relies on empirical Lennard-Jones parameters, which were taken from the CHARMM force field.[S17] The best agreement with experiment was found with a tip lateral spring constant of about 0.5 N/m, similar to values reported in previous studies.[S18] All other parameters are the same as intended by Hapala *et al.*, and the simulated AFM scan is performed at a resolution of 5 pm (in all directions), with a force tolerance criterion of 4×10^{-6} eVÅ^{-1}. The 3D force field is subsequently converted into a frequency shift image,[S19] using the experimental parameters.

Simulated nc-AFM image of $DCBP_3Co_2$ MOF

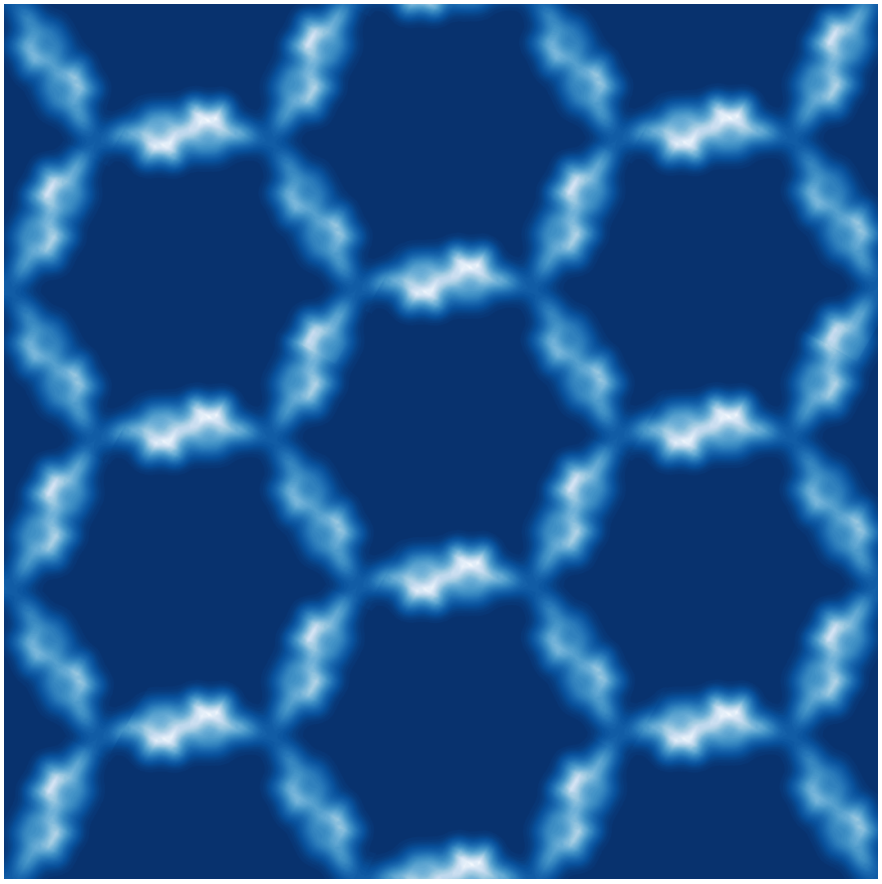

Figure S1: Simulated nc-AFM image of DFT optimized $DCBP_3Co_2$ MOF shows non-planarity of DCBP molecules and the chirality exhibited by the framework.

Large area image of DCA_3Co_2 MOF

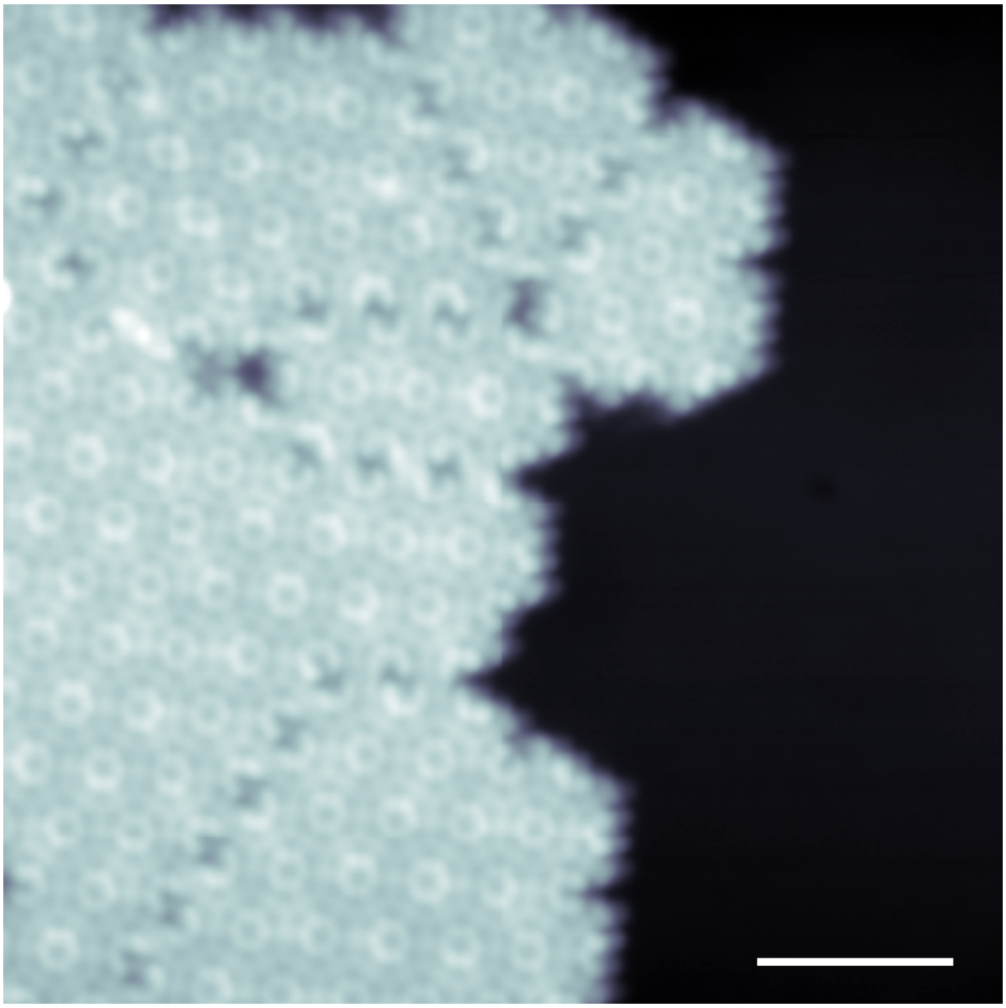

Figure S2: A large area STM image of DCA_3Co_2 MOF on G/Ir(111) surface (dark area) showing various domains of different sizes. The scale bar is 5 nm and the imaging parameters are $V = 1.3$ V and $I = 20$ pA.

Co-N bond lengths

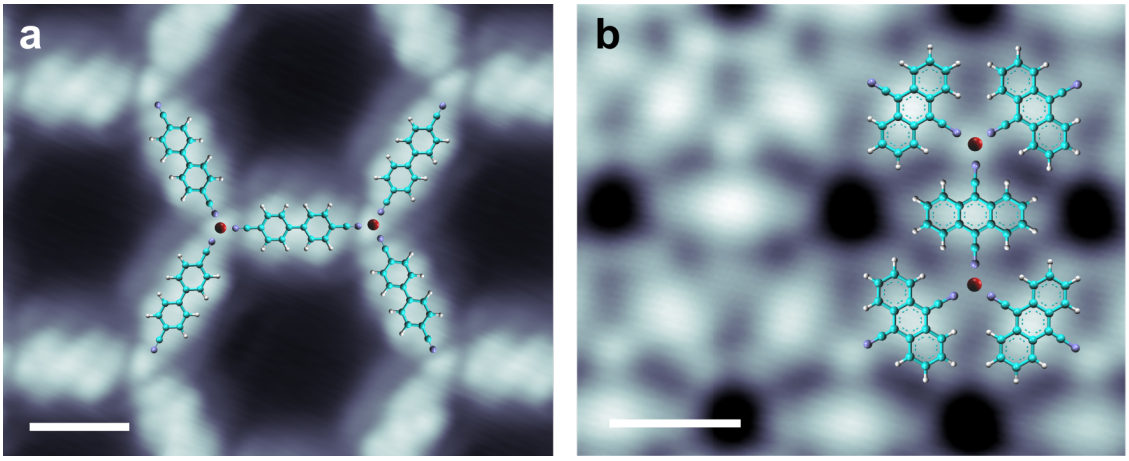

Figure S3: Scaled molecular structures are overlaid on the STM topography image of (a) $DCBP_3Co_2$ and (b) DCA_3Co_2 MOFs. From here, we extract Co-N bond to be 1.5 ±0.2Å. Scale bars are 10 Å.

k

Assembly of DCA_3Co single complexes on G/Ir(111)

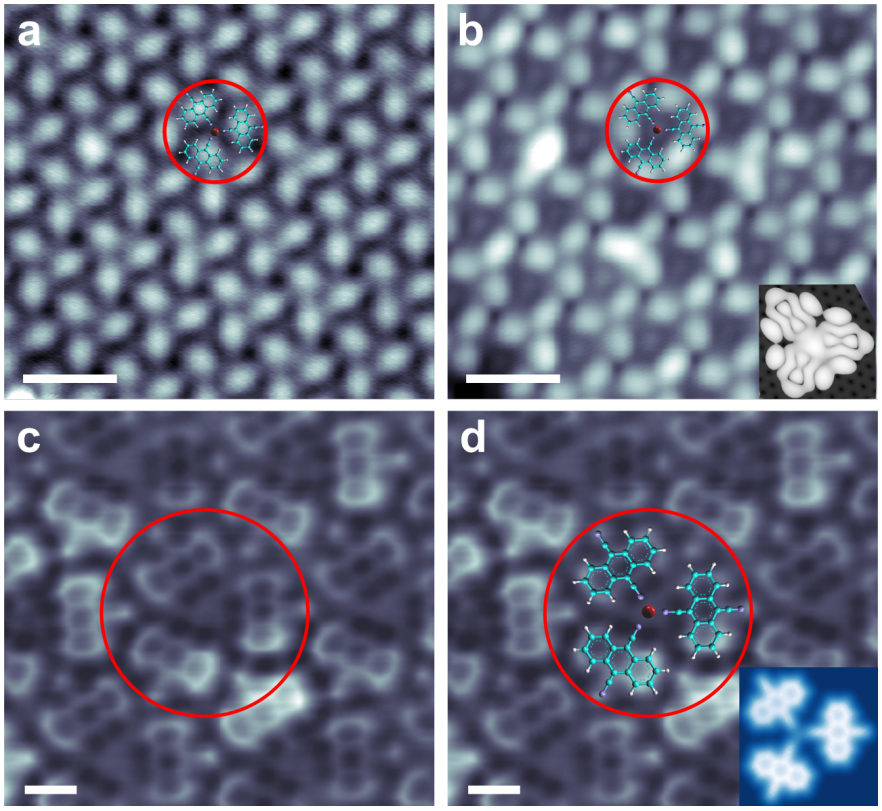

Figure S4: (a) A large scale STM image of DCA_3Co single complex assembly recorded at bias, $V = 0.3$ V ($I = 2$ pA) showing the backbone of DCA molecules. The red circle indicates a single complex on the surface. The scale bar is 2 nm. (b) An STM image of the same area at bias $V = 0.8$ V ($I = 2$ pA) shows LUMO of the DCA molecules and cobalt at the center of the complex. The red circle indicates the same complex indicated in panel a. The inset shows DFT simulated STM image of DCA_3Co complex showing LUMO. (c) An nc-AFM image of a zoomed-in area shows internal structure of the molecules and their arrangement in the single complex assembly. Again, the red circle indicates a single complex. The cyano groups bonded to cobalt atom are lower than the non-bonded cyano groups. Cobalt atom is not visible at this tip height. (d) Same as panel c with an overlaid chemical structure of the DCA_3Co single complex. The inset shows a simulated nc-AFM image of the single complex.

Bias dependent STM imaging of DCBP molecule, $DCBP_4Co$ single complex, and $DCBP_3Co$ stripe-phase

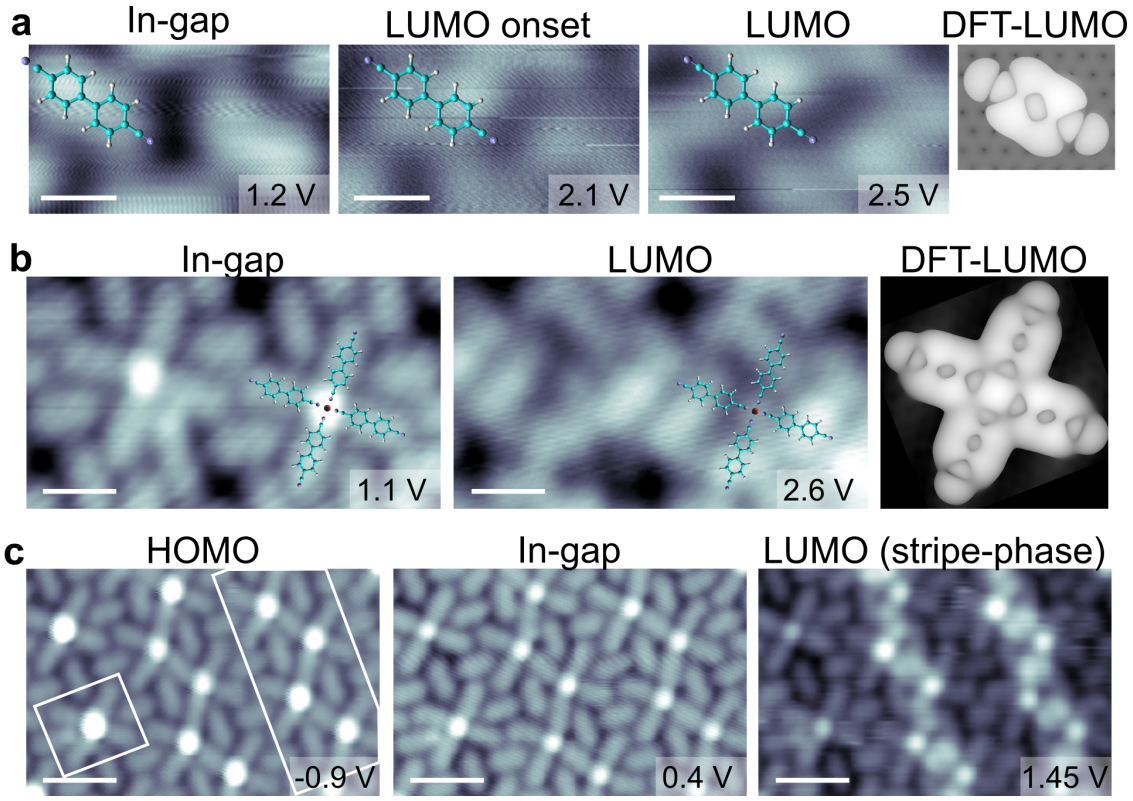

Figure S5: (a) Bias dependent STM topography images of the same area contains DCBP molecules showing backbone (1.2 V), LUMO onset (2.1 V) and LUMO (2.5 V) and DFT simulated STM image showing LUMO. Scale bars are 5 Å. (b) Bias dependent STM image of the same area contains $DCBP_4Co$ single complex showing backbone (1.1 V) and LUMO (2.6 V) and DFT simulated STM image depicting LUMO. Scale bars are 1 nm. (c) Bias dependent STM images of $DCBP_4Co$ single complex and $DCBP_3Co$ stripe showing HOMO (-0.9 V) with a bright cobalt center, in-gap image (0.4 V), and LUMO of $DCBP_3Co$ stripe-phase (1.45 V). Scale bars are 2 nm. In the STM image, LUMO of DCBP appears as if the backbone has rotated with respect to the molecular long axis owing to finite torsional angle between the phenyl rings of the DCBP molecule. This is visible for DCBP molecule in the molecular assembly, the single complexes, and the stripe phase.

Distance dependent gating on DCBP LUMO due to cobalt atoms

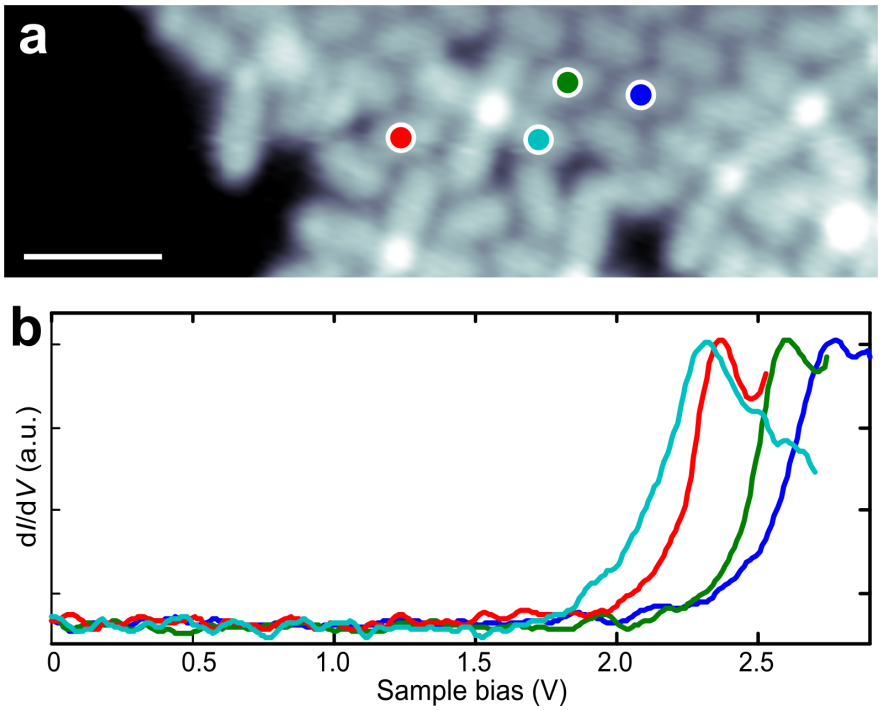

Figure S6: (a) STM image of a mixed island of DCPB molecules and $DCPB_4Co$ complexes. The scale bar is 2 nm. Sample bias, $V = 0.77$ V and setpoint, $I = 0.7$ pA. (b) Gating effect on the DCPB LUMO due to the presence of cobalt metal atoms on the surface. dI/dV spectra are compared for DCBP molecules lying at various distances from the cobalt metal atoms: DCBP molecule far away from the cobalt atoms has LUMO peak at 2.75 V (blue curve) which is very close to the LUMO peak in close-packed molecular assembly. The LUMO peak shifts to 2.60 V (green curve) for a DCBP molecule close to a $DCBP_4Co$ single complex. For another non-bonded DCBP molecule, close to two single complexes, the peak shifts to 2.37 V (red curve). A representative spectrum (cyan curve) on DCPB molecule bonded to a $DCBP_4Co$ single complex has a LUMO peak at 2.30 V.

Assembly of DCA molecules on G/Ir(111)

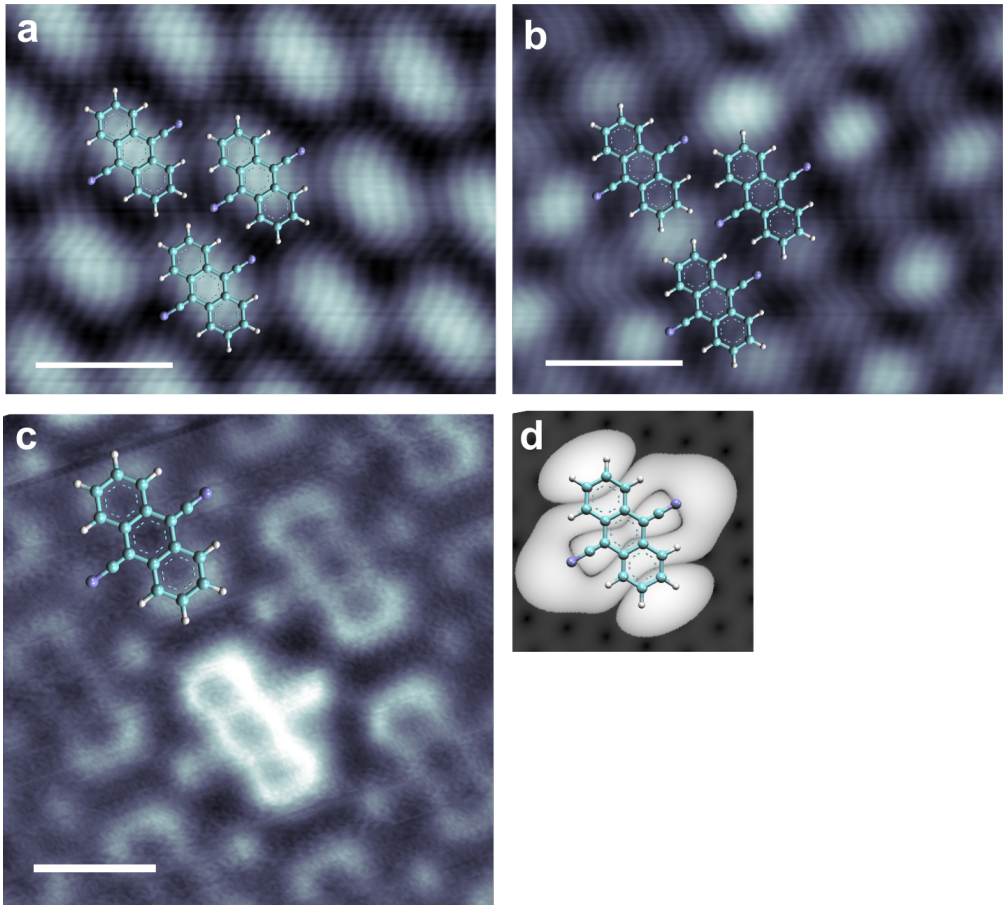

Figure S7: DCA molecule forms close-packed assembly on G/Ir(111) surface. (a) STM topography image of DCA molecules at in-gap sample bias V = 0.4 V (I = 1.5 pA) shows molecular backbone. The scale bar is 1 nm. (b) STM topography image of the same area as **a** recorded at 1.6 V (I = 1.5 pA) shows LUMO of the DCA. The LUMO of DCA has one lobe at each end of the anthracene long axis which is consistent with earlier report[S20] and DFT simulated LUMO of DCA as in **d**. The scale bar is 1 nm. (c) A zoomed-in nc-AFM image of molecular assembly reveals the structure of the DCA molecules and their arrangement. The scale bar is 5 Å. (d) DFT simulated STM image of DCA depicting LUMO. Molecular structures are overlaid on each image for the clarity.

dI/dV spectrum on Co in $DCBP_3Co_2$ MOF

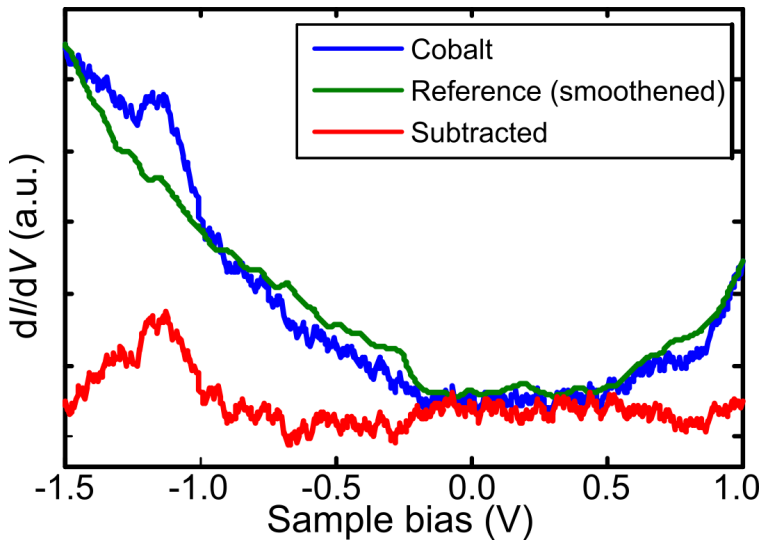

Figure S8: dI/dV spectrum (blue curve) on Co in $DCBP_3Co_2$ MOF shows a faint peak at -1.15 V. After subtracting the reference dI/dV spectrum (green curve) recorded on G/Ir(111) surface, we extract the spectrum on Cobalt (red curve).

High spatial-resolution dI/dV spectra on DCA_3Co_2 honeycomb MOF

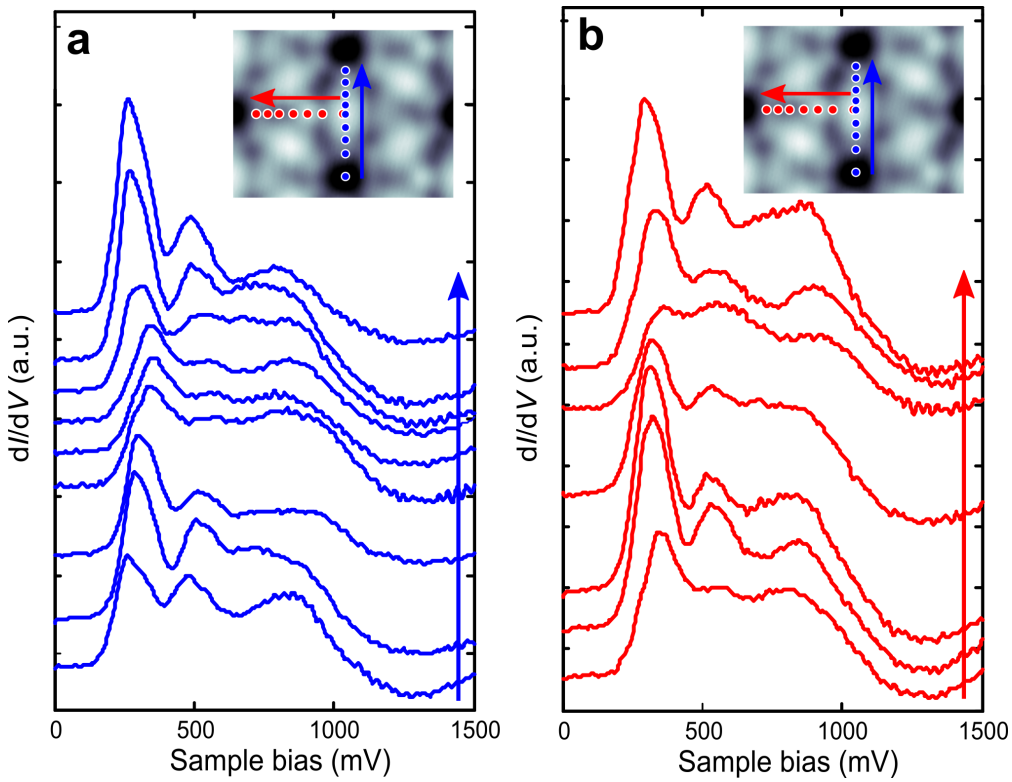

Figure S9: (a,b) dI/dV point spectra recorded along the backbone of DCA (panel a) and across cobalt atom (panel b) of DCA_3Co_2 MOF as shown in the insets. At the center of the ring of DCA lobes, dI/dV spectra shows peak position at 260 mV which shifts to 290 mV at the position of the lobe which further shifts to 350 mV at the center of the molecule. Across the cobalt atom, the peak position shifts to 320 mV from 350 mV at the center of DCA. Inset imaging parameters $V = 120$ mV and setpoint $I = 33$ pA.

dI/dV spectra on DCA_3Co single complex with DCA_3Co_2 honeycomb MOF

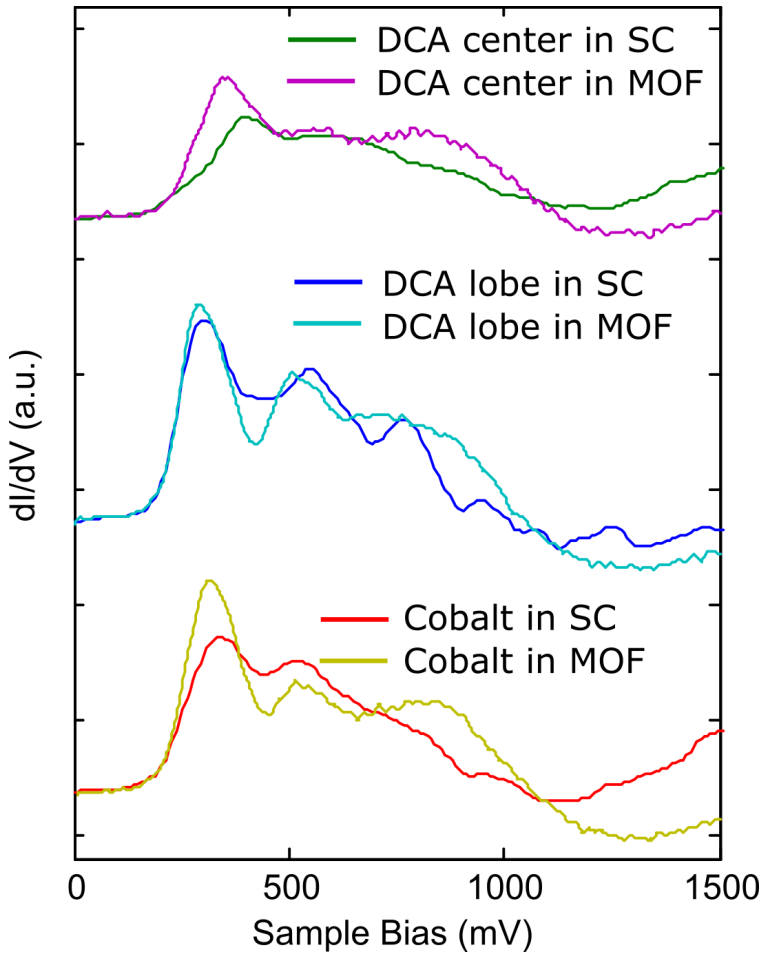

Figure S10: dI/dV point spectra comparison between DCA_3Co single complex (SC) and DCA_3Co_2 MOF. The spectra at various locations of MOF are displaced vertically w.r.t each other for visualization and the respective SC spectra are vertically displaced too to match MOF spectra. Further, each SC spectrum is shifted towards fermi energy by 470 mV and multiplied by various factors to achieve approximate normalization. Spectra at DCA center, DCA lobe, and cobalt of SC was multiplied by 2.5, 2.7 and 3.1, respectively. Each spectrum recorded on MOF show enhanced NDR effect, due to further decoupling from the substrate as in $DCBP_3Co_2$ MOF. Despite enhanced decoupling, there is at least an excess of states at energies higher than 700 mV.

DFT simulated band structure of DCA_3Co_2 MOF with and without graphene

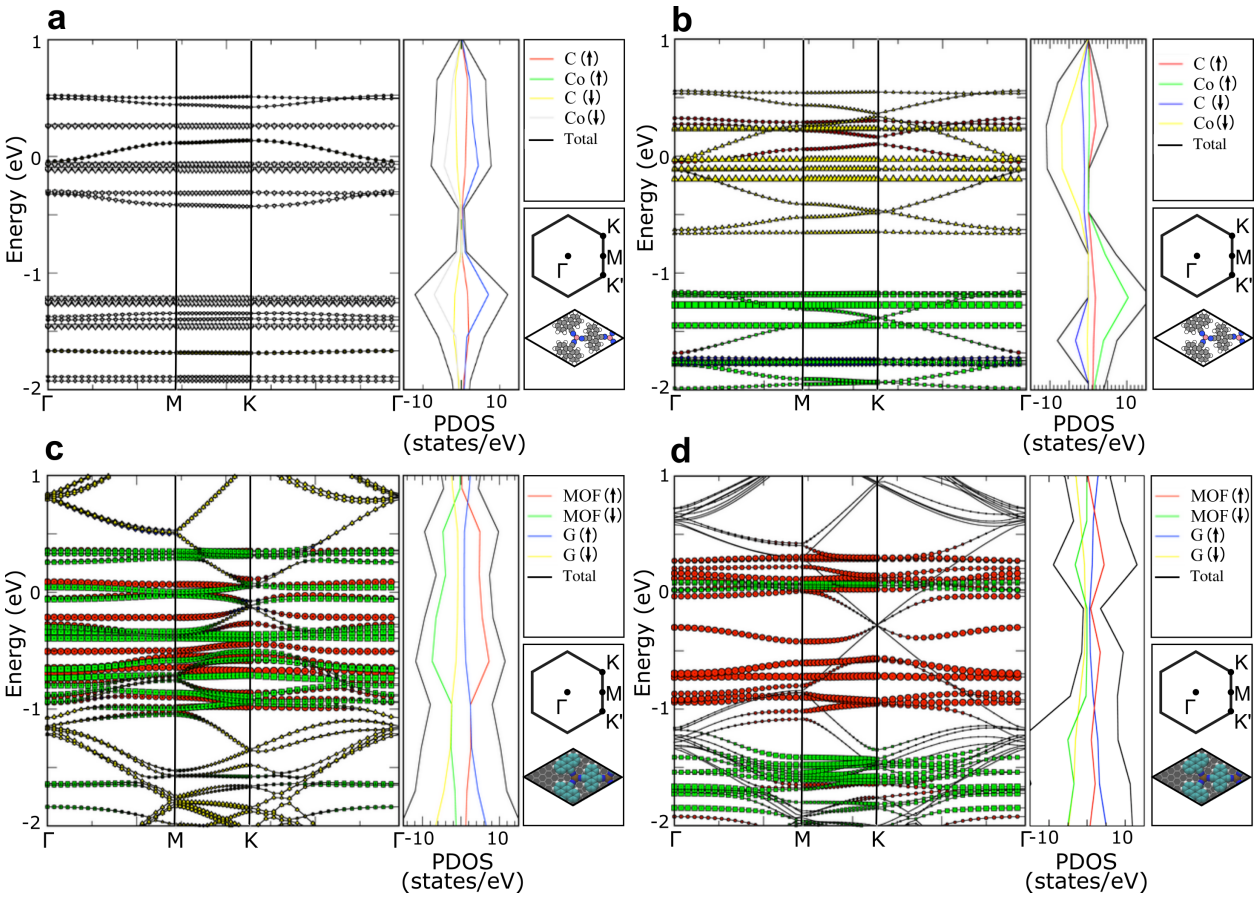

Figure S11: Band structure of DCA_3Co_2 MOF with and without graphene. The top panels (a) and (b) show gas phase MOF band structure for antiferromagnetic and ferromagnetic configurations, respectively, while the bottom panels, (c) and (d) are the corresponding band structures for the MOF adsorbed on graphene. The band structures on the graphene look complicated due to the additional bands arising from the graphene and the slight shifts and splittings of the MOF states due to the interaction with the graphene. The slight shifts of the MOF bands with energy is the result of charge transfer between the MOF and graphene. However, it can be seen that the MOF derived bands are not strongly affected by the underlying graphene.

Band structure and LDOS maps of DCA_3Co_2 MOF for the antiferromagnetic ground state

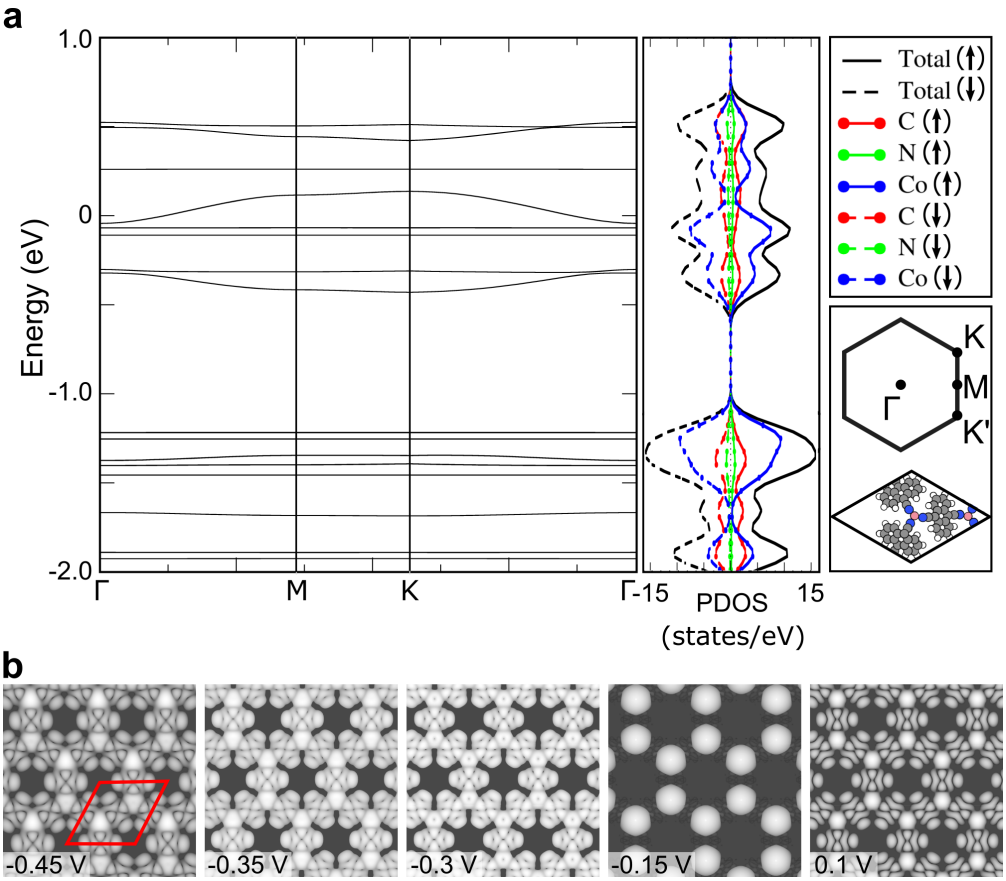

Figure S12: (a) Calculated band structure of DCA_3Co_2 MOF for the antiferromagnetic ground state. The band structure shows a number of gaps at Γ-point and smaller gaps at K-point which is inconsistent with the measured dI/dV spectra. While, the top right panels show the partial density of states, the bottom panel shows the unit cell and corresponding Brillouin zone. Presence of a large gap between -0.4 eV and -1.25 eV in the calculated band structure and no observation of states below Fermi energy in the dI/dV spectra until -1.5 V suggests that the energy corresponding to the experimental Fermi level will lie below the flat band at energy -0.3 V. (b) Simulated LDOS maps for the similar energy range as in measured dI/dV band width shows the LDOS map deviates significantly at -0.15 V from the measured dI/dV maps. The red rhombus represents the unit cell of the structure.

dI/dV spectra at the edges of $DCBP_3Co_2$ MOF domain

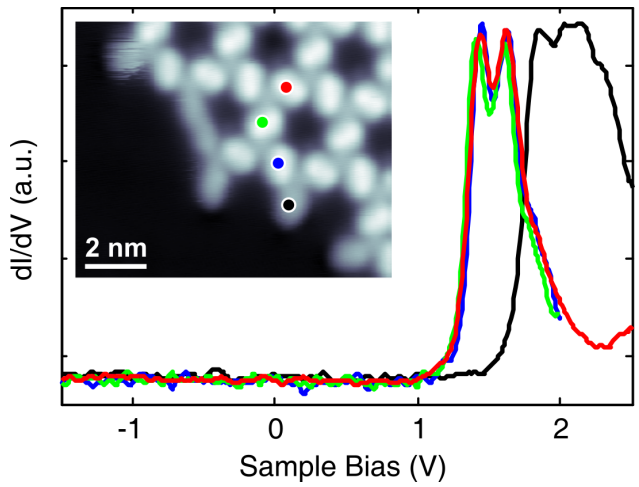

Figure S13: Comparison of the dI/dV spectra recorded on DCBP molecules at different locations of a $DCBP_3Co_2$ domain. Spectrum recorded on a DCBP molecule at the edge (black curve) shows that DCBP LUMO is located at 1.8 V. However, dI/dV spectrum recorded on the next DCBP molecule (blue curve) already looks comparable to that measured in the interior of the domain (green and red curves). Inset imaging parameters: 1.3 V and 1 pA. Scale bar is 2 nm.

dI/dV spectra at the edges of DCA_3Co_2 MOF domain

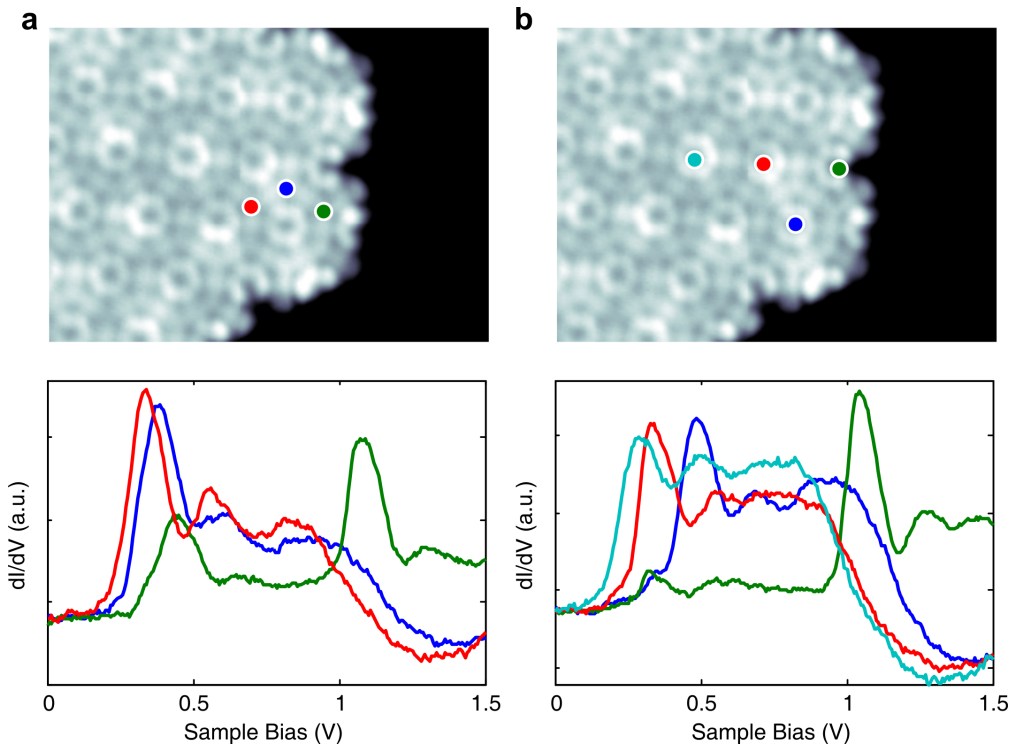

Figure S14: Comparison of the dI/dV spectra recorded on different locations of a DCA_3Co_2 domain. (a) dI/dV spectrum recorded on a cobalt site at the edge (green curve) shows superposition of two bands: shifted band at higher energy and bands from the interior. dI/dV spectrum (blue curve) recorded on the next cobalt atom already looks comparable to that from the interior of the domain (red curve). (b) Similarly, dI/dV spectrum recorded at the center of honeycomb at the edge shows superposition of two bands: shifted band at higher energy and the band from the interior. dI/dV spectrum (blue curve) recorded on the center of the honeycomb at the corner still shows a weak gating effect. dI/dV spectrum (red curve) recorded at the center of the honeycomb next to the edge already looks comparable to that from the interior of the domain (cyan curve). Imaging parameters: 1.5 V and 23 pA. The scale bar is 2 nm.

References

(S1) Gross, L.; Mohn, F.; Moll, N.; Liljeroth, P.; Meyer, G. *Science* **2009**, *325*, 1110–1114.

(S2) Horcas, I.; Fernández, R.; Gómez-Rodríguez, J. M.; Colchero, J.; Gómez-Herrero, J.; Baro, A. M. *Rev. Sci. Instrum.* **2007**, *78*, 013705.

(S3) `http://gwyddion.net/`.

(S4) Nečas, D.; Klapetek, P. *Cent. Eur. J. Phys.* **2012**, *10*, 181–188.

(S5) Kresse, G.; Furthmüller, J. *Comp. Mat. Sci.* **1996**, *6*, 15.

(S6) Kresse, G.; Furthmüller, J. *Phys. Rev. B* **1996**, *54*, 11169.

(S7) Klimeš, J.; Bowler, D. R.; Michaelides, A. *J. Phys. Condens. Matter* **2010**, *22*, 022201.

(S8) Klimeš, J.; Bowler, D. R.; Michaelides, A. *Phys. Rev. B* **2011**, *83*, 195131.

(S9) Björkman, T.; Gulans, A.; Krasheninnikov, A.; Nieminen, R. M. *Phys. Rev. Lett.* **2012**, *108*, 235502.

(S10) Blöchl, P. E. *Phys. Rev. B* **1994**, *50*, 17953.

(S11) Zhang, L. Z.; Wang, Z. F.; Huang, B.; Cui, B.; Wang, Z.; Du, S. X.; Gao, H.-J.; Liu, F. *Nano Lett.* **2016**, *16*, 2072–2075.

(S12) Dudarev, S. L.; Botton, G. A.; Savrasov, S. Y.; Humphreys, C. J.; Sutton, A. P. *Physical Review B* **1998**, *57*, 1505–1509.

(S13) Mann, G. W.; Lee, K.; Cococcioni, M.; Smit, B.; Neaton, J. B. *The Journal of Chemical Physics* **2016**, *144*, 174104.

(S14) Vanpoucke, D. E. P.; Brocks, G. *Phys. Rev. B* **2008**, *77*, 241308.

(S15) Hapala, P.; Temirov, R.; Tautz, F. S.; Jelinek, P. *Phys. Rev. Lett.* **2014**, *113*, 226101.

(S16) `https://github.com/SINGROUP`.

(S17) Brooks, B. R. et al. *J. Comput. Chem.* **2009**, *30*, 1545–1614.

(S18) Hapala, P.; Kichin, G.; Wagner, C.; Tautz, F. S.; Temirov, R.; Jelinek, P. *Phys. Rev. B* **2014**, *90*, 085421.

(S19) Welker, J.; Illek, E.; Giessibl, F. J. *Beilstein J. Nanotechnol.* **2012**, *3*, 238–248.

(S20) Liljeroth, P.; Swart, I.; Paavilainen, S.; Repp, J.; Meyer, G. *Nano Lett.* **2010**, *10*, 2475–2479.